Chapter 1

Babcock-Leighton dynamos

1.1 The Babcock-Leighton mechanism [S6BL]

In 1961 Horace W. Babcock proposed an empirical model for the solar cycle based on the decay of large bipolar active evolution, and their contribution to the evolution of the sun's surface poloidal magnetic field. Further elaborated by R. Leighton in the late 1960's, the model was soon largely displaced by dynamo models based on then newly elaborated mean-field electrodynamics theory, and lay more or less dormant for over two decades. It only recently re-emerged as a full fledged contender in the quest for an explanatory model of the solar cycle.

1.1.1 The decay of bipolar active regions

Figure 1.1.1 illustrates the basic idea of the Babcock-Leighton mechanism. Consider the two bipolar magnetic regions (BMR) sketched on part (A). Recall that each of these is the photospheric manifestation of a toroidal flux rope eemrging as an Ω-loop. The *leading* (*trailing*) component of each BMR is that located ahead (behind) in the direction of the Sun's rotation (from E to W). Joy's Law (§X.Y) states that, on average, the leading component is located at lower latitude than the trailing component, so that a line joining each component of the pair makes an angle with respect to the E-W line. Hale's polarity law also inform us that the leading/trailing magnetic polarity pattern is opposite in each hemisphere, a reflection of the equatorial antisymmetry of the underlying toroidal flux system.

Babcock demonstrated empirically from his observation of the sun's surface solar magnetic field that as the BMRs decay (presumably under the

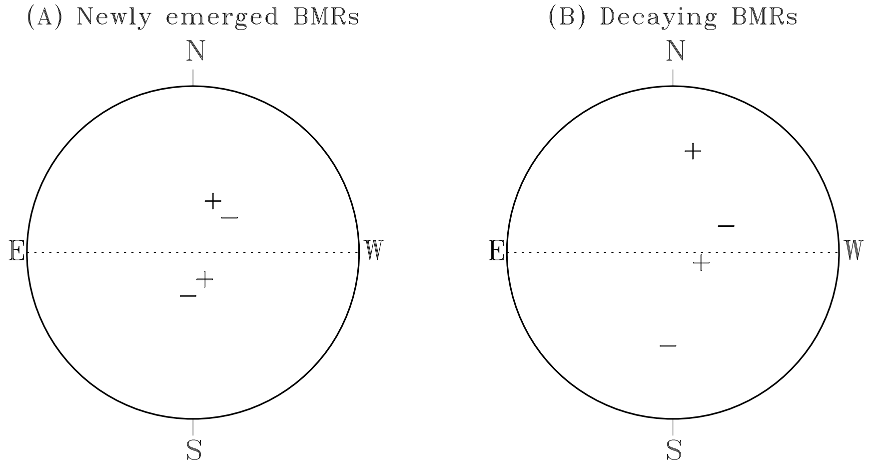

Figure 1.1: [F6.1] Cartoon of the Babcock-Leighton mechanism. On the left, two bipolar magnetic regions (BMR) have emerged, one in each hemisphere, with opposite leading/following polarity patterns, as per Hale's polarity Law. After some time the BMRs have decayed, the leading components have reconnected across the equator, while the trailing components have moved to higher latitudes. The net effect is the buildup of an hemispheric flux of opposite polarity in the N and S hemisphere, i.e., a net dipole moment (see text).

influence of turbulent convection), the trailing components drift to higher latitudes, leaving the leading components at lower latitudes, as sketched on Fig. 1.1.1B. Babcock also argued that the trailing polarity poloidal flux released to high latitude by the cumulative effects of the emergence and subsequent decay of many BMRs was responsible for the reversal of the sun's large-scale dipolar field. More germane from the dynamo point of view, the Babcock-Leighton mechanism taps into the (formerly) toroidal flux in the BMR to produce a poloidal magnetic component. Recall from §**??** that this is the part of the dynamo cycle that was problematic from the point of view of Cowling's theorem.

To the degree that a positive dipole moment is being produced from a toroidal field that is positive in the N-hemisphere, this is a bit like a positive α-effect in mean-field theory. In both cases the Coriolis force is the agent imparting a twist on a magnetic field; with the α-effect this process occurs on the small spatial scales and operates on individual magnetic fieldlines. In contrast, the Babcock-Leighton mechanism operates on the large scales, the twist being imparted via the the Coriolis force acting on the flow generated along the axis of a buoyantly rising magnetic flux tube (see §III.X.Y).

The first of many refs. to flux tube part

1.1.2 An illustrative numerical simulation

Evidently this mechanism can operate as sketched on Figure 1.1.1 provided the magnetic flux in the leading and trailing components of each (decaying) BMR are separated in latitude faster than they can diffusively cancel with one another. Moreover, the leading components must end up at low enough latitudes for diffusive cancellation to take place acros the equator. This is not trivial to achieve, and we now take a more quantitative looks at the Babcock-Leighton mechanism, first with a simple 2D numerical model.

The starting point of the model is the grand sweeping assumption that, once the sunspots making up the bipolar active region lose their cohesiveness, their subsequent evolution can be approximated by the passive advection and resistive decay of the radial magnetic field component. This drastic simplification does away with any dynamical effect associated with magnetic tension and pressure within the spots, as well as any anchoring with the underlying toroidal flux system. The model is further simplified by treating the evolution of B_r as a two-dimensional transport problem on a spherical surface corresponding to the solar photosphere. Consequently, no subduction of the radial field can take place.

Even under these simplifying assumptions, the evolution is still governed by the MHD induction equation, specifically its r-component. The imposed flow is made of an axisymmetric "meridional circulation" and differential rotation:

$$\mathbf{u}(\theta) = 2u_0 \sin\theta\cos\theta\hat{\mathbf{e}}_\theta + \Omega_S(\theta)R\sin\theta\hat{\mathbf{e}}_\phi \ , \tag{1.1}$$

where Ω_S is the surface differential rotation profile used in the preceeding chapter (see eq. (**??**)). Note that $\nabla\cdot\mathbf{u} \neq 0$, a direct consequence of working on a spherical surface without possibility of subduction. Introducing a new latitudinal variable $\mu = \cos\theta$ and neglecting all radial derivatives, the r-component of the induction equation (evaluated at $r = R$) becomes:

$$\frac{\partial B_r}{\partial t} = \frac{2u_0}{R}(1-\mu^2)\left[B_r + \mu\frac{\partial B_r}{\partial\mu}\right] - \Omega_S(1-\mu^2)^{1/2}\frac{\partial B_r}{\partial\phi}$$

$$+\frac{\partial}{\partial\mu}\left[\frac{\eta}{R^2}\frac{\partial B_r}{\partial\mu}\right] + \frac{\partial}{\partial\phi}\left[\frac{\eta}{R^2(1-\mu^2)}\frac{\partial B_r}{\partial\phi}\right] \ , \tag{1.2}$$

with η being the magnetic diffusivity. As usual, we work with the nondimensional form of eq. (1.2), obtained by expressing time in units of $\tau_{\rm u} = R/u_0$, i.e., the advection time associated with the meridional flow. This leads to the appearance of the following two nondimensional numbers in the scaled version of eq. (1.2):

$$\mathrm{R}_m = \frac{u_0 R}{\eta} \ , \qquad \mathrm{R}_u = \frac{u_0}{\Omega_0 R} \ . \tag{1.3}$$

Using $\Omega_0 = 3 \times 10^{-6}\,\mathrm{rad\ s}^{-1}$, $u_0 = 1500\,\mathrm{cm\,s}^{-1}$, and $\eta = 6 \times 10^{12}\,\mathrm{cm}^2\,\mathrm{s}^{-1}$ yields $\tau_{\rm u} \simeq 1.5\,\mathrm{yr}$, $\mathrm{R}_m \simeq 20$ and $\mathrm{R}_u \simeq 10^{-2}$. The former is really a measure of the (turbulent) magnetic diffusivity, and is the only free parameter of the model, as R_u is well constrained by surface Doppler measurements. The corresponding magnetic diffusion time is $\tau_\eta = R^2/over\eta \simeq 26\,\mathrm{yr}$, so that $\tau_{\rm u}/\tau_\eta \ll 1$.

Figure 1.1.2 shows a representative solution. The initial condition (panel A, $t=0$) mimics a series of eight BMRs, four per hemisphere, equally spaced 90^o apart at latitudes $\pm 30°$. Each BMR consists of two Gaussian profiles of opposite sign and adding up to zero net flux, with angular separation $d = 10°$ and with a line joining the center of the two Gaussians tilted with respect to the E-W direction[1] by an angle γ, itself related to the latitude θ_0 of the BMR's midpoint according to the Joy's Law-like relation

$$\sin\gamma = 0.5\cos\theta_0 \tag{1.4}$$

The symmetry of the initial condition means that the problem can be solved in a single hemisphere with $B_r = 0$ enforced in the equatorial plane, in a 90° wide longitudinal wedge with periodic boundary conditions in ϕ.

The combined effect of circulation, diffusion and differential rotation is to concentrate the magnetic polarity of the trailing "spot" to high latitude, while the polarity of the leading spot remains near the original location of the active region. This is readily seen upon calculating the longitudinally averaged latitudinal profiles of B_r, as shown on Fig. 1.1.2F for the five successive epochs shown on (A)—(E). This is essentially equivalent to Babcock's original cartoon (cf. 1.1.1). The time required to achieve this here is $t/\tau_{\rm u} \sim 1$, and scales[2] as $(\mathrm{R}_m/\mathrm{R}_u)^{1/3}$.

[1]Remember that this is meant to represent the result of a toroidal flux rope erupting through the surface, so that in this case the underlying toroidal field is positive, which is the polarity the polarity of the trailing "spot", as measured with respect to the direction of rotation, from left to right here.

[2]Can you figure that one out?

We can use these simulation results to estimate the "efficiency" of the Babcock-Leighton mechanism. First we define the mean signed and unsigned magnetic flux:

$$\Phi =\mid \langle B_r \rangle \mid \ , \qquad F = \langle \mid B_r \mid \rangle \ , \tag{1.5}$$

where the averaging operator on the spherical surface is simply

$$\langle B_r \rangle = -\int_0^{2\pi} \int_{-1}^{+1} B_r \mathrm{d}\mu \mathrm{d}\phi \ . \tag{1.6}$$

Figure 1.1.2A shows the time-evolution of the signed and unsigned flux F, for the solution of Fig. 1.1.2. The unsigned flux decreases rapidly at first, then settles into a slower decay phase[3]. Meanwhile a small but significant hemispheric signed flux is building up. This is a direct consequence of (negative) flux cancellation across the equator, mediated by diffusion, and is the Babcock-Leighton mechanism in action. Note the dual, conflicting role of diffusion here; it is needed to for cross-hemispheric flux cancellation, yet must be small enough to allow the survival of a significant trailing polarity flux on timescales of order τ_{u}.

The efficiency (Ξ) of thre Babcock-Leighton mechanism, i.e., converting toroidal to poloidal field, can defined as the ratio of the signed flux at $t = \tau_{\mathrm{u}}$ to the BMR's initial unsigned flux[4]:

$$\Xi = 2\frac{\Phi(t = \tau_{\mathrm{u}})}{F(t = 0)} \ . \tag{1.7}$$

Note that Ξ is independent of the assumed initial field strength of the BMRs since eq. (1.2) is linear in B_r. The efficiency does depend on the tilt and separation of the initial bipolar region, and on the adopted values for R_u and R_m (You get to explore this in Problem 6.X!). Figure 1.1.2B shows the variation of Ξ with BMR latitudinal location, for $\mathrm{R}_m = 10$, 20 and 100. The efficiency is highest for BMRs initially located at high latitudes, even though the tilt γ is smaller. This is because proximity to the equator favors transequatorial diffusive fluxcancellation of the leading component, while having $\mathrm{d}u_\theta/\mathrm{d}\theta < 0$ favors the separation of the two BMR components, thus minimizing diffusive flux csncellation between the leading and trailing components. The efficiency does depend non-trivially on many of the model's parameters,... something you get to explore further in Problem 6.1!

[3]This should remind you of something encountered a few chapter ago...

[4]Can you figure out why a factor of two was inserted on the RHS of eq. (1.7?

1.1.3 Axisymmetrization revisited

Take another look at Fig. 1.1.2; at $t = 0$ (panel A) the surface magnetic field distribution is highly non-axisymmetric. By $t/\tau_\mathrm{u} = 0.5$ (panel E), however, the field distribution shows a far less pronounced ϕ-dependency, especially at high latitudes where in fact B_r is nearly axisymmetric. This should remind you of something we encountered earlier: axisymmetrization of a non-axisymmetric magnetic field by an axisymmetric differential rotation (§2.YY), the spherical analog of flux expulsion (§2.XX). In fact a closer look at the behavior of the unsigned flux on Fig. 1.1.2A (dashed line) shows the two-timescale behavior we have come to expect of axisymmtrrization: the rapid destruction of the non-axisymmetric flux component and slower ($\sim \tau_\eta$) diffusive decay of the remaining axisymmetric flux distribution.

Since the spherical harmonics represent a complete and nicely orthonormal functional basis on the sphere, it follows that the initial condition for the simulation of Fig. 1.1.2 can be written as

$$B_r^0(\theta,\phi) = \sum_{l=0}^{\infty} \sum_{m=-l}^{+l} b_{lm} Y_{lm}(\theta,\phi) \tag{1.8}$$

or just refer to Tom's appendix?

where the Y_{lm}'s are the spherical harmonics:[5]

$$Y_{lm}(\theta,\phi) = \sqrt{\frac{2l+1}{4\pi}\frac{(l-m)!}{(l+m)!}} P_l^m(cos\theta) e^{im\phi} \ , \tag{1.9}$$

and with the coefficients b_{lm} given by

$$b_{lm} = \int_0^{2\pi} \int_0^{\pi} B_r^0(r,\theta) Y_{lm}^*(\theta,\phi) \tag{1.10}$$

where the "$*$" indicates complex conjugation[6]. Now, axisymmetrization will wipe all $m \neq 0$ modes, leaving only the $m = 0$ modes to decay away on the slower diffusive timescale[7]. Therefore, at the end of the axisymmetrization process, the radial field distribution now has the form:

$$B_r(\theta) = \sum_{l=0}^{\infty} \sqrt{\frac{2l+1}{4\pi}} b_{l0} P_l(\cos\theta) \ , \qquad t/\tau_\mathrm{u} \gg \mathrm{R}_u \ . \tag{1.11}$$

[5]Better rewrite those factorials differently when trying a numerical implementation...

[6]What are the non-zero b_{lm} for the inclined dipole treated in §X.Y?

[7]With $\mathbf{u} = 0$, the decay rate of those remaining modes are given by the eigenvalues of the 2D pure resistive decay problem, much like in §2.XX [THIS COULD BE A PROBLEM IN CHAP. IV.2].

FIGURE: b_{lm} gray scale plot, with resulting asymptotic $B_r(\theta)$, and corresponding $\langle B_r \rangle$ from above simulation. [8]

1.2 A Babcock-Leighton solar cycle model [S6sol]

All fine, but how are we to make a a solar cycle-like model of the Babcock-Leighton mechanism? It does take care of the toroidal→poloidal half of the dynamo loop. We still have differential rotation to do the poloidal→toroidal part, so in principle we're in good shape. There's a complication, however; the strongest shear resides in the tachocline, around the core-envelope interface, while the Babcock-Leighton mechanism is a surface effect. If we want to make a working dynamo these two source regions need to "communicate" with one another. Meridional circulation is a prime candidate for this crucial role.

Figure 1.2 illustrates schematically the mode of operation of a Babcock-Leighton dynamo. Let's begin with a high latitude poloidal field, at location s_1. Circulation carries this poloidal field down into the envelope (s_2) and equatorward more or less along the core-envelope interface, where the strong radial shear induces a strong toroidal component at s_3. This toroidal field forms flux ropes, which rise radially to the surface at s_4. As we saw in the preceding section, the combined action of differential rotation, circulation and diffusion is to produce a more or less axisymmetric surface poloidal field concentrated at high latitude, effectively bringing us back to s_1 and to the close the dynamo loop

There are many possible ways to formulate mathematically a dynamo model based on the Babcock-Leighton mechansm[9] To date all models have retained the assumption of axisymmetry for the large-scale field, in which case we can use our usual poloidal/toroidal decomposition with the poloidal component expressed in terms of a toroidal vector potential (see eq. (**??**)), and write down something resembling in fact the $\alpha\Omega$ dynamo equations including meridional circulation:

$$\frac{\partial A}{\partial t} = \eta \left(\nabla^2 - \frac{1}{\varpi^2} \right) A - \frac{1}{\varpi} \mathbf{u}_p \cdot \nabla(\varpi A) + S(r, \theta, B) \ , \qquad (1.12)$$

[8]How would you go about computing the toroidal-to-poloidal efficiency factor Ξ within this modeling framework?

[9]The model and numerical results described in the remainder section are taken directly from the paper by Dikpati & Charbonneau (1999) listed in the bibliography, where references to other modeling approaches can also be found.

$$\frac{\partial B}{\partial t} = \eta\left(\nabla^2 - \frac{1}{\varpi^2}\right)B - (\nabla\eta)\times(\nabla\times\mathbf{B})$$

$$-\varpi\nabla\cdot\left(\frac{B}{\varpi}\mathbf{u}_p\right) + \varpi(\nabla\times A)\cdot(\nabla\Omega)\ . \tag{1.13}$$

The source term S on the RHS of eq. (1.12), a (nonlinear) function of the toroidal field B, will soon come to describe poloidal field regeneration by the Babcock-Leighton mechanism[10]. For the differential rotation and meridional circulation we simply retain the analytic forms described in the previous chapter (see Figs. **??** and **??**)[11], as well our now familiar error function profile for the magnetic diffusivity, with $\Delta\eta = 10^{-3}$ (see eq. (**??**).

As with the mean-field dynamo equations, nondimensionalization of eq. (1.12)—(1.13) leads to the appearance of three dimensionless quantities C_S, C_Ω and R_m (cf. eqs. (**??**)—(**??**)), the latter two identical to the mean-field case and the first, $C_S = s_0 R/\eta_0$, now measuring the strength of the Babcock-Leighton source term relative to dissipation.

1.2.1 Formulation of the poloidal source term

The definition of the Babcock-Leighton source term S in eq. (1.12) is evidently the crux of the model. Consider the following:

$$S(r,\theta,B(t)) = s_0 f(r)\sin\theta\cos\theta\left[1-\left(\frac{B(r_c,\theta,t)}{B_0}\right)^2\right]^{-1} B(r_c,\theta,t)\ , \tag{1.14}$$

$$f(r) = \frac{1}{2}\left[1+\mathrm{erf}\left(\frac{r-r_2}{d_2}\right)\right]\left[1-\mathrm{erf}\left(\frac{r-r_3}{d_3}\right)\right] \tag{1.15}$$

where s_0 is a numerical coefficient setting the strength of the source term (corresponding dynamo number being $C_S = s_0 R/\eta_0$), and with the various remaining numerical coefficient taking the values $r_2/R = 0.95$, $r_3/R = 1$, $d_2 = d_3 = 10^{-2}R$, and $B_0 = 10^5$ G. Note that the dependency on B is *non-local*, i.e., it involves the toroidal field evaluated at the core-envelope interface

[10] Note that setting $S = \alpha B$ would take us back to the mean-field model considered in §5.XX, namely the $\alpha\Omega$ dynamo with meridional circulation.

[11] The forthcoming numerical results, taken directly from Dikpati & Charbonneau (1999), use in fact a meridional circulation profile that, although similar to that plotted on Fig. **??**), is different in details. This is inconsequential in the present context.

r_c, (but at the same colatitude θ). The combination of error functions concentrate the source term immediately beneath the surface, which is fine. The nonlocality in B represents the fact that the strength of the source term is proportional to the field strength in the bipolar active region, itself presumably reflecting the strength of the diffuse toroidal field near the core-envelope interface, where the magnetic flux ropes eventually giving rise to the bipolar active region originate (see §III.X.Y). The nonlocal quenching nonlinearity reflects the fact that as the strength of the flux rope reaches about 10^5 G, the flux rope emerges without the tilt essential to the Babcock-Leighton mechanism. The $\cos\theta$ dependency is a first order description of Joy's Law, i.e., the tilt of active regions increases with latitude. Notably missing in eq. (1.14) is some sort of lower threshold on S, to mimic the fact that flux ropes with field strengths lower than a few tens of kG either fail to be destabilized in a short enough timescale (§III.X.X), rise to the surface at high latitudes and without systematic tilt patterns (§III.X.Y), and/or fail altogether to survive their rise through the convective envelope (§III.X.Z). Also missing is some sort of sink term in eq. (1.13), to take into account the loss of toroidal flux associated with the formation and destabilization of a strong toroidal flux rope.

Ref to part III

More refs. to part III

The nonlocality of S notwithstanding, at this point the model equations are definitely mean-field like. Yet no averaging on small scales is involved. What is implicit in eq. (1.14) is some sort of averaging process at least in longitude and time.

1.2.2 A solar-like solution

We focus here on one specific solar-like dynamo solution with parameter values $u_0 = 1500\,\mathrm{cm\,s^{-1}}$, $s_0 = 20\,\mathrm{cm\,s^{-1}}$, and $\eta = 3\times10^{11}\,\mathrm{cm^2\,s^{-1}}$, leading to $C_\Omega = 47000$, $C_S = 4.64$, and $\mathrm{R}_m = 348$. Equations (1.12) and (1.13) are solved as an initial-boundary value problem using a weak random field as initial condition. After transients have damped out, the model settles in a oscillatory mode with the field amplitude limited by the B_0 value adopted in eq. (1.14).

Butterfly diagrams for the core-envelope interface toroidal field and surface radial component are shown in Fig. 1.2.2, which should be compared with the corresponding diagrams obtained for our "best" mean-field model (Fig. **??**). The solution has a reasonable toroidal butterfly diagram, and the phase relationship between poloidal and toroidal fields is in agreement with observations. The solution is also characterized by a predominance of negative magnetic helicity in the N-hemisphere, and has a peak field strength of 10.4 kG at the core-envelope interface. Its peak surface polar field strength, about 140 G, is roughly a factor of ten too high[12].

One aspect of this solution is particularly noteworthy, namely its period: 19.8 years. Moreover, for this model the dynamo period T has been shown to scale as

$$T = 56.8 u_0^{-0.89} s_0^{-0.13} \eta_0^{0.22} \qquad [\mathrm{yr}] \ , \tag{1.16}$$

With the circulation flow speed constrained by helioseismology, the observed solar cycle period is a rather tight constraint for dynamo models of the Babcock-Leighton variety, unlike with mean-field models where the period is readily tuned by adjusting the magnetic diffusivity, a notoriously difficult quantity to estimate observationally or theoretically.

this is at least as good as the best mean-field model of the preceding chapter!

1.3 Effects of stochastic fluctuations

The source term used above represents some sort of average over the decay of many tilted bipolar active regions, distributed in longitude, latitude, and time. Consequently, statistical fluctuations about the mean are bound to occur. In addition, we must consider fluctuations in the meridional circulation. The latter is a weak flow most likely driven by Reynolds stresses and slow compared to turbulent velocities themselves. The prospect of circulation being strongly fluctuating is potentially dangerous for Babcock-Leighton model, since circulation is crucially needed to couple the surface and core-envelope interface, i.e., the two source regions in the model.

We consider below two distinct, yet complementary approaches to the fluctuation problem. The first is a straight numerical simulation based on the DC99 model, and the second is based on a reduction of the dynamo equations to an iterative map.

[12]This is actually a common difficulty with Babcock-Leighton model, and arises from the fact that meridional circulation converges to the pole, so that magnetic flux conservation requires an increase in field strength to offset the shrinking surface element.

1.3.1 A numerical simulation

[13]

Starting from the model of the preceding section, we now introduce stochastic fluctuations in both the source term and meridional circulation. For the source term we simply set

$$s_0 \to s_0 + s'\sigma(t;\tau_c) \tag{1.17}$$

where τ_c is a (specified) *coherence time* during which the fluctuation $s'\sigma$ is held constant at value determined by the quantity σ, itself extracted from a sequence of random deviates uniformly distributed in the interval $[-1, 1]$. The ratio s'/s_0 then becomes a measure of the peak fluctuation amplitude.

For the circulation care must be taken to maintain mass conservation in the fluctuating flow. This can be achived via the definition of a spatially random, time-dependent stream function $\Psi(r, \theta, t; \tau_c)$, so that

$$\mathbf{u}_p \to \mathbf{u}_p + \frac{u'}{\rho r \sin\theta}\left[\frac{1}{r}\frac{\partial \Psi}{\partial \theta}\hat{\mathbf{e}}_r - \frac{\partial \Psi}{\partial r}\hat{\mathbf{e}}_\theta\right] \tag{1.18}$$

with $\Psi = 0$ enforced at the domain boundaries (for further implementation details, see the paper by Charbonneau and Dikpati listed in the bibliography). The ratio u'/u_0 is then a measure of the peak fluctuation amplitude in the circulation.

Figure 1.3.1 shows result for a strongly fluctuating run with $s'/s_0 = 2$, $u'/u_0 = 1$, and $\tau_c = 1\,$month. Part (A) is a butterfly diagram for the toroidal field at the core-envelope interface, and part (B) a time series of B^2 extracted along the dotted line on part (A). Evidently the dynamo has no difficulty operating more or less normally even in this strongly fluctuating regime.

The time series plotted on Fig. 1.3.1 can be taken as a proxy of sunspot number, allowing to extract simulated cycle half-periods P_n and amplitudes A_n from the simulation[14]. Figure 1.3.1A shows the resulting period-amplitude correlation plot; it is solar-like, in that it shows an *anticorrelation* between cycle amplitude and period, at a statistically weak yet still significant level. Moreover, the overall spread in cycle period is comparable to that characterizing sunspot data (see Fig. **??**). Not bad!

[13] The numerical results discussed in this section are taken directly from the Charbonneau & Dikpati (2000) paper listed in the bibliography.

[14] This should be a reasonably safe procedure in the case of the cycle period. On the other hand, much is missing in our current understanding of a flux rope formation from a diffuse field, and sunspt formation from an emerging flux rope, so that the "cycle amplitude" obtained here cannot be compared in detail with sunspot data.

Using the sequence of cycle amplitudes A_n, one can compute a 1-2-1 running mean

$$\langle A_n \rangle = \frac{1}{4}(A_{n-1} + 2A_n + A_{n+1}) \tag{1.19}$$

and computed a detrended sequence $A_n - \langle A_n \rangle$; the result is shown on Fig. 1.3.1B. Note the recurrent epochs where the cycle amplitude alternate between lower- and higher-than-average (emphasized by thicker lines on Fig. 1.3.1B). This is qualitatively similar to the so-called odd-even effect seen in sunspot data (cf. Fig. **??**).

Short paragraph on clock properties.

1.3.2 A dynamical system approach

We now turn to a totally different approach to the study of fluctuations in Babcock-Leighton dynamos, emphasizing from the onset the importance of long time delay[15]. The time delay is associated with the finite time required for meridional circulation to carry the poloidal field produced in the surface layer by the decay of bipolar active regions, down to the shear layer at the core-envelope interface.

Let T_n, P_n be the amplitudes of the toroidal and poloidal magnetic fields at cycle n. Our starting point is the realization that the production of the toroidal magnetic field T_{n+1} at cycle $n+1$ in the shear layer at the core-envelope interface is proportional to the surface poloidal magnetic field P_n of the *preceding* cycle. Go back to Fig. 1.2 and consider the coordinate s defined along a meridional circulation streamlime threading poleward through the surface layer and equatorward at the core-envelope interface (outermost streamline on Fig. 1.2). The time interval Δt required to go from s_1 to s_3 is

$$\Delta t = \int_{s_1}^{s_3} \frac{\mathrm{d}s}{u(s)} \simeq \frac{s_3 - s_2}{u} \;, \tag{1.20}$$

where the second approximate equality follows from the fact that the circulatory flow is much slower at at base of the envelope than higher up, and where $u \equiv \langle u_\theta(r_c, \theta) \rangle$ is now an average latitudinal flow speed evaluated at r_c. We also do away with magnetic dissipation as well as induction within the envelope itself. Clearly this implies $P_n(s_2) = P_n(s_1)$. Further assuming

[15] "long" here means comparable to the cycle length. The model discussed in §1.2 and used in §1.3.1 above is indeed characterized by such a time delay.

that the poloidal field is being acted upon by a constant rotational shear $\Delta\Omega$ in the course of its journey from s_2 to s_3, the toroidal field strength at s_3 is then simply

$$T_{n+1} = (\Delta\Omega)(\Delta t)P_n \ . \tag{1.21}$$

In keeping with the Babcock-Leighton picture, the production of the poloidal field at s_4 is assumed to be a function of the toroidal field of the current cycle (at s_3), in some proportion to the amplitude of the toroidal field:

$$P_{n+1} = f(T_{n+1})T_{n+1} \ , \tag{1.22}$$

where $f(T_{n+1})$ is an as-yet unspecified function measuring the efficiency of the Babcock-Leighton mechanism as a function of the toroidal field strength in the shear layer. Let now $\bar{P}$, $\bar{T}$ be representative values for the poloidal and toroidal field amplitudes, and introduce dimensionless field amplitude variables $p_n = P_n/\bar{P}$, $t_n = T_n/\bar{T}$. Equation (1.21) implies $\bar{T}/\bar{P} = \Delta\Omega\Delta t$, so that eqs. (1.21) and (1.22) become:

$$t_{n+1} = p_n \ , \tag{1.23}$$

$$p_{n+1} = (\bar{T}/\bar{P})f(t_{n+1})t_{n+1} \ , \tag{1.24}$$

Substituting the former in the latter yields

$$p_{n+1} = (\bar{T}/\bar{P})f(p_n)p_n \ , \tag{1.25}$$

This expression is known by mathematicians as a one-dimensional parametric iterative map (hereafter just “map”, for brevity's sake). It is an iteration algorithm that allows the calculation of successive cycle amplitudes, given an initial cycle amplitude p_0. However, we cannot do a thing with it until we come up with a function $f(t_n)$... which is supposed to embody all the physics of the Babcock-Leighton mechanism, from the destabilization of thin flux ropes, rise through the envelope, emergence with a tilt, and final surface decay! We'll pick a extremely simple form for $f(t_n)$, but not quite totally arbitrarily. Simulations of rising thin flux ropes described in chapter X of part III indicate that for toroidal field strengths in excess of about 100 kG, flux ropes emerge parallel to the E-W direction, i.e., without the tilt that is essential to the Babcock-Leighton mechanism. In addition, we also learned that for toroidal field strengths below about 10 kG the flux ropes emerge at high latitudes and with tilt patterns incompatible with Joy's Law. Moreover, it turns out that such weak flux ropes are easily randomized by stochastic buffeting associated with the turbulent fluid motions in the convective envelope, and might not even survive their buoyant rise through the envelope. This implies that the Babcock-Leighton mechanism is characterized by both lower and upper operating thresholds. It also suggests that poloidal field production decreases faster than t_n as the toroidal field falls below 10 kG or so. Perhaps the simplest analytic form capturing this behavior is

$$f(t_n;\gamma) = (\bar{P}/\bar{T})\gamma\, t_n(1-t_n)\ , \qquad \gamma > 0\ , \tag{1.26}$$

where γ is a control parameter measuring the efficiency of the Babcock-Leighton mechanism, so that eq. (1.25) becomes

$$p_{n+1} = \gamma\, p_n^2(1-p_n)\ , \qquad [\ \equiv g(p_n;\gamma)\ ]\ , \qquad \gamma > 0\ . \tag{1.27}$$

Evidently this map admits the two solutions

$$p_n \equiv \mu_0 = 0\ , \qquad \forall\gamma\ , \tag{1.28}$$

$$p_n \equiv \mu_1 = \frac{1 \pm \sqrt{1-4/\gamma}}{2}\ , \qquad \gamma \geq 4\ . \tag{1.29}$$

This is intuitively appealling; finite amplitude cycles (i.e., $p_n > 0$) are only possible beyond a certain critical value of the control parameter γ, which, as per eq. (1.26) is a measure of the strength of the Babcock-Leighton mechanism, and so plays the role of a dynamo number. The critical value $\gamma = 4$ then becomes the analog of the critical dynamo number!

Solutions of the form $p_{n+1} = p_n$ are called *fixed points.* For γ not too large (more on this very soon!), and starting from any $p_0 \neq \mu_0, \mu_1$, an amplitude iterate sequence will always converge to either μ_0 or μ_1. The ensemble of initial conditions p_0 for which the map will converge to one or the other fixed points defines the *basin of attraction* of each fixed point.

Life is just not that simple, however. In general, one-dimensional maps such as that defined Equation (1.27) also admit *limit cycle* solutions, i.e., solutions of the form

$$p_{n+m} = p_n\ , \qquad p_{n+k} \neq p_n\ , \qquad m > 1 \text{ and } 1 < k < m\ . \tag{1.30}$$

where m denotes the *period* of the limit cycle. Indeed, it can be shown that the nontrivial fixed point solution loses stability to a period-2 limit cycle when

$$\frac{\mathrm{d}g(p_n;\gamma)}{\mathrm{d}p_n}\Big|_{p_n=\mu} \leq -1 \ . \tag{1.31}$$

Denote by λ_1 the value of γ at which this takes place; for the map defined by eq. (1.27), you can easily verify that $\lambda_1 = 16/3$. As γ is further increased the period-2 limit cycle eventually loses stability (at $\gamma = \lambda_2$) to a period-4 limit cycle, which later becomes unstable to a period-8 limit cycle (at $\gamma = \lambda_3$), and so on, in a manner reminiscent of Zeno's paradox. This process of *bifurcation* is best viewed by plotting successive values of p_n against γ, after disappearance of any transient associated with the choice of p_0. Figure 1.3.2 shows the bifurcation diagram generated in this manner for eq. (1.27). The various branches represent stable solutions, in that the p_n iterates always return to those stable values if artificially perturbed. Collectively, they define the *attractor* of the dynamical system. Examination of the bifurcation diagram also reveals that something peculiar seems to be happening beyond $\gamma \gtrsim 5.9$. Successive iterates fill an ever-widening p_n range, and this time small external perturbations are amplified exponentially as the iteration proceed For $\gamma \gtrsim 5.9$, eq. (1.27) exhibits *chaotic behavior*. Finally, for $\gamma \geq 6.5433$ the trivial solution is again the only stable solution.

There is something truly unique to the attractor's bifurcation diagram: it is *universal* to one-dimensional maps characterized by a single critical point, i.e., "single hump" maps $g(p_n)$ for which $\mathrm{d}g/\mathrm{d}p_n = 0$ for one and only one p_n in the maps' range. Whatever the functional form of $g(p_n)$, the transition to chaos always proceeds through the same geometric sequence of bifurcations through period-2^m limit cycles, with $m = 1, 2, ...$ Moreover, it can be shown that, for all sufficiently steep one-dimensional single hump maps,

$$\lim_{n\to\infty} \frac{\lambda_{n-1}-\lambda_n}{\lambda_n-\lambda_{n+1}} = \delta = 4.669201... \tag{1.32}$$

where the universal constant δ is known as Feigenbaum's number. One great practical advantage to eq. (1.32) is that it provides a recurrence relation allowing to calculate the value λ_∞ at which transition to chaos takes place, from measurement of the first few bifurcation points. This yields $\lambda_\infty = 5.8878...$ for the bifurcation diagram plotted in Fig. 1.3.2.

OK, so this is all nice and cute, but can we learn anything from this about the solar cycle? It turns out that this type of modeling has direct bearing on at least one aspect of observed solar cycle fluctuations discussed in §**??**: the odd-even effect in cycle amplitude. Consider the behavior of the amplitude iterates when the control parameter γ lies in the range $5.333 \leq \gamma \leq 5.7635$, corresponding to the period-2 limit cycle regime on Fig. 1.3.2. Successive amplitude iterates alternate betwen the upper and lower stable branch, i.e., the subsequence of iterates p_{2n} is higher than average (say), and the complementary sequence p_{2n+1} is lower than average. This is qualitatively similar to the odd-even effect observed in sunspot numbers between cycles 9 to 22. But are we not relying here on a rather fine tuning of the map's control parameter? It turns out that this explanation of the odd-even effect is rather robust, materializing as it does in stochastically forced versions of eq. (1.27. Consider for example the stochastically forced map defined by

$$p_{n+1} = \gamma_n p_n^2 (1 - p_n) + \varepsilon_n \ , \tag{1.33}$$

where the map's parameter γ_n is now drawn anew at each iteration from a sequence of random deviate uniformly distributed in some preset interval $[\gamma_1, \gamma_2]$. Similarly, ε_n is drawn from a separate sequence of random deviate distributed in $[0, \varepsilon]$, with $\varepsilon \ll 1$. This map is thus subjected to both multiplicative and additive noise, yet shows a strong odd-even signal even when the interval $[\gamma_1, \gamma_2]$ is as wide as the window of non-trivial behavior on Fig. 1.3.2. Figure 1.3.2A shows a portion of an iterate sequence for eq. (1.33) with $\gamma_n \in [4.5, 6.5]$ and $\varepsilon_n \in [0, 0.09]$. Figure 1.3.2B shows a detrended version of Fig. 1.3.2A, obtained by subtracting a 1-2-1 running mean (solid line on part A) from the sequece itself, as done with the sunspot amplitude data on Fig. **??**. Even with such strong fluctuations, the odd-even effect shows up quite clearly. How can this be, given that with this level of stochastic forcing γ_n lies outside the interval $[\lambda_1, \lambda_2]$ for about 88% of iterations? The explanation lies with the fact that, at fixed γ, the convergence to the corresponding fixed point or limit cycle is often oscillatory, so that the fluctuating map responds in an "overstable" manner to the stochastically varying γ_n.

Stochastic forcing has yet another potentially interesting consequence, namely pushing the iterate sequence in or out of the attraction basin of the trivial solution, leading to *intermittency*, i.e., it alternates between quiescent phases with $p_n \sim \varepsilon$, and bursting phases with $p_n \sim 1$. A similar behavior has been observed in other one-dimensional maps, and at this point we simply refer the interested reader to problem X.Y, as well as the papers listed in the bibliography, for further detail on intermittency in general, and its mode of operation in the context of the map defined by eq. (1.27).

1.4 Chaos, stochasticity and the solar cycle

It is of course tempting to identify quiescent phases on Fig. 1.3.2C with periods of strongly reduced solar activity, such as the Maunder minimum, but caution is definitely in order here. there are many alternative ways to produce such epochs of supressed activity in reduced

---

Problems:

1. This problem get's you to explore the efficiency of the Babcock-Leighton mechanism by numerically solving yourself the 2D surface evolution problem of §1.1.2. Proceed as follows:
   (a) Introduce a new variable $b = B_r/sin\theta$ in eq. (1.2), and obtain the corresponding non-dimensional evolution equation for b.
   (b) Write a code to solve this equation numerically using second-order centered finite differences and explicit single-step time-stepping. Be careful to consider both the advection and diffusion terms in computing the Courant condition for the time step size. Check your code by trying to reproduce the solution of Fig. 1.1.2.
   (c) Now you're all set to study the dependence of the Babcock-Leighton efficiency factor Ξ on (do only *one* of the following):
      i. the separation d of the leading/trailing BMR components, at fixed latitude θ_0 and tilt angle γ;
      ii. the tilt angle γ of the BMR, at fixed latitude θ_0 and component separation d;
      iii. the meridional flow speed u_0, at fixed latitude θ_0, tilt γ, and separation d.
2. Now you get to try a different procedure to compute the efficiency factor Ξ. First obtain an expression for Ξ in terms of the expansion coefficients b_{lm}; next write yourself a numerical code to carry out the spherical harmonic decomposition for the initial condition used in §1.1.2; once this is done (and tested), study the dependence of Ξ on
   (a) the separation d of the leading/trailing BMR components, at fixed latitude θ_0 and tilt angle γ;

(b) the tilt angle γ of the BMR, at fixed latitude θ_0 and component separation d;

(c) the meridional flow speed u_0,

3. This problem let's you develop a dynamo-inspired map, and study its behavior along the lines followed in §1.3.2. Your starting point is the set of two coupled equations introduced in §1.2, and describing field amplification in Babcock-Leighton dynamos.

   (a) Obtain a one-dimensional map corresponding to the non-local α-quenching nonlinearity introduced in eq. (**??**). This is actually simpler than you might think...

   (b) Construct a bifurcation diagram for this map, and calculate the value of the fixed point as a function of your map's control parameter. Does the trivial solution retain a finite basin of attraction? Where does transition to a period-2 limit cycle take place? The transition to chaos?

   (c) Examine now the behavior of a stochastically forced version of your map without additive noise, i.e., iterate the map while extracting your control parameter anew at each iteration from a sequence of random deviate uniformly distributed in some interval $[0, \Sigma]$. Does your forced map exhibit intermittency? If so, what is the intermittency threshold on Σ?

   (d) Examine the sequence of amplitude iterates in the stochastically forced version of your map. Does it exhibit something resembling the odd-even effect?

Bibliography:

What is now refered to as Babcock-Leighton solar-cycle models go back to the following two seminal papers by H. Babcock and Leighton:

Babcock, H.W. 1961, *Astrophys. J.*, **133**, 572,
Leighton, R.B. 1964, *Astrophys. J.*, **140**, 1547,
Leighton, R.B. 1969, *Astrophys. J.*, **156**, 1.

Although some details of the model are different, the 2D surface simulations described in §1.1.2 basically follow

Wang, Y.-M., Nash, A.G., & Sheeley, N.R. Jr 1991, *Science*, **245**, 712,
Wang, Y.-M., & Sheeley, N.R. Jr 1991, *Astrophys. J.*, **375**, 761,

For 3D model for the evolution of the Sun's poloidal field, see

Dikpati, M., & Choudhuri, A.R. 1995, *Solar Phys.*, **161**, 9,
Choudhuri, A.R., & Dikpati, M. 1999, *Solar Phys.*, **184**, 61.

The Babcock-Leighton dynamo model described in §1.2 is taken directly from

Dikpati, M., & Charbonneau, P. 1999, *Astrophys. J.*, **518**, 508.

For different modeling approaches, see

Wang, Y.-M., & Sheeley, N.R. Jr, & Nash, A.G. 1991, *Astrophys. J.*, **383**, 431,
Durney, B.R. 1995, *Solar Phys.*, **160**, 213,
Durney, B.R. 1996, *Solar Phys.*, **XXX**, YYY,
Durney, B.R. 1997, *Astrophys. J.*, **486**, 1065.
Choudhuri, A.R., & Nandy, D. 2001, ApJin press?.

The latter paper, in particular, explores the correspondence between Durney's discrete eruption approach, and the mean-field-like formulation used in §1.2. In this general context, see also

Choudhuri, A.R., Schüssler, M., & Dikpati, M. 1995, A&A309L29.

Most of the results for stochastically fluctuating models described in §1.3.1 are taken directly from

Charbonneau, P., & Dikpati, M. 2000, *Astrophys. J.*, **543**, 1027.

Section 1.3.2 is based on

Durney, B.R. 2000, *Solar Phys.*, **in press**, YYY.
Charbonneau, P. 2001, *Solar Phys.*, **in press**, YYY.

The reduction of the Babcock-Leighton dynamo equations to a one-dimensional map follows the first of these papers, while the subsequent analysis follows the second, where stochastic forcing and intermittency in dynamo-inspired one-dimensional maps are discussed at greater depth than in §1.3.2. On intermittency see also

Platt, N., Spiegel, E.A., & Tresser, C. 1993, *Phys. Rev. Lett.*, **70**, 279
Heagy, J.F., Platt, N., & Hammel, S.M.: 1994, *Phys. Rev. E*, **49**, 1140

The universal character of single-hump one-dimensional maps was first investigated in detail in the landmark paper

Feigenbaum, M.J. 1978, *J. Stat. Phys.*, **19**, 25

but for a more accessible introduction to one-dimensional maps consult first

Holton, D., & May, R.M. 1993, *Chaos and one-dimensional maps*, in *The Nature of Chaos*, ed. T. Mullin (Oxford: Oxford University Press), p. 69.

The literature on chaos in physical systems is immense. The following is our (very biased and probably not exceedingly well-informed) list of "top-five" chaos papers or books, based on usefulness, level-headedness, and/or physical insight:

Lorenz, E.N. 1963, *J. Atmos. Sci.*, **20**, 130
Mullin, T. (ed.), *The Nature of Chaos*,

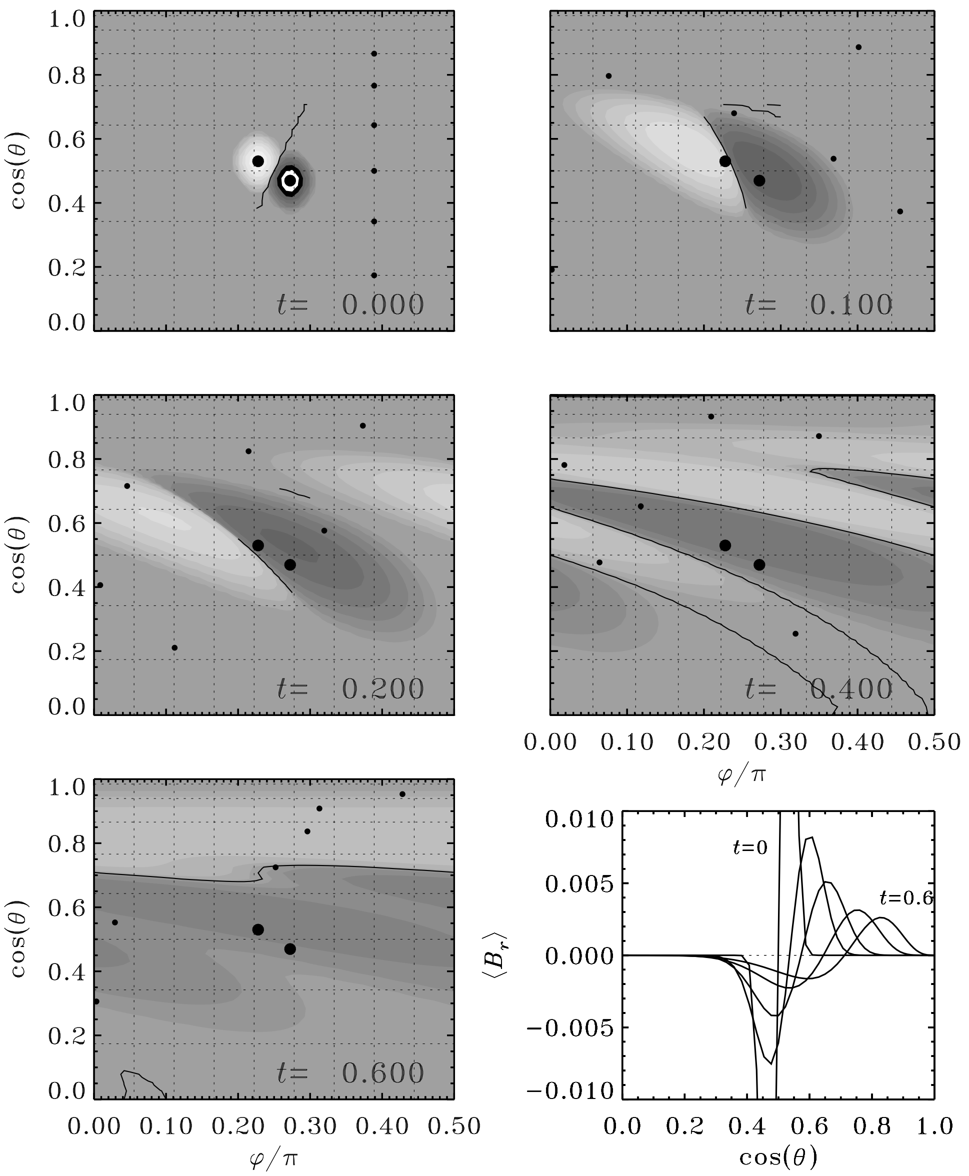

Figure 1.2: [F6.2] The first five panels show the evolution of the surface radial magnetic field component, as described by the 2D advection-diffusion equation (1.2). Parameter values are $\mathrm{R}_u = 10^{-2}$ and $\mathrm{R}_m = 50$ [MAYBE]. Time is given in units of the circulation turnover time $\tau_{\mathrm{u}} = R/u_0$. Note how after only half a turnover time the high latitude magnetic field is already very axisymmetric. The bottom right panel shows the evolution of the longitudinally averaged radial magnetic field.

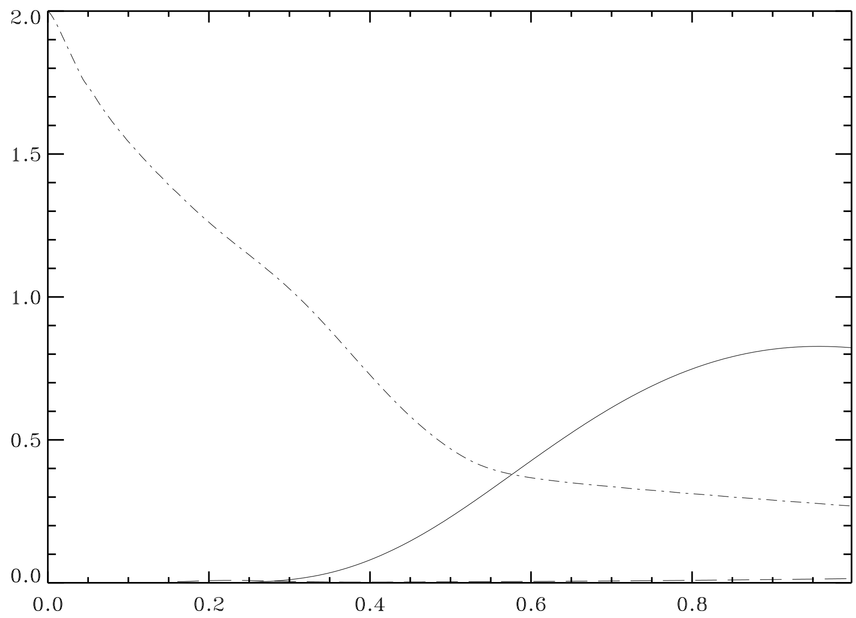

Figure 1.3: [F6.3] Evolution of the signed (solid line) and unsigned (dashed line) magnetic flux for the advection-diffusion solution of Fig. 1.1.2. Note the rapid initial decay of the unsigned flux, followed by a slower decay phase.

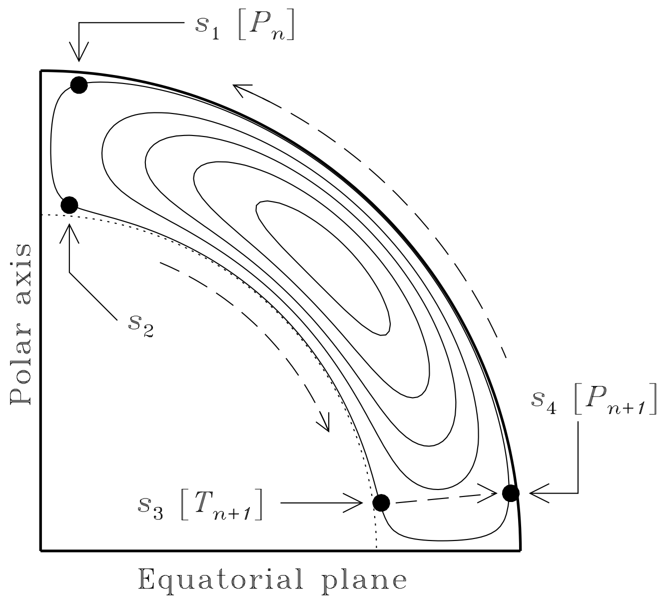

Figure 1.4: [F6.4] Schematic representation of the magnetic field amplification and transport process in Babcock-Leighton dynamos. The high latitude surface poloidal field P_n at s_1 is advected by meridional circulation downward to s_2 and equatorward to s_3, in the course of which it experiences shearing by differential rotation, so that a toroidal field is produced, reaching maximal amplitude T_{n+1} at s_3. Eruption of that toroidal field from s_3 to s_4, followed by the subsequent decay of the tilted bipolar region, leads to the production of a new poloidal field P_{n+1} at s_4, which is then advected poleward, so that the the next field amplification cycle is now ready to start. The finite ime required for the field to be transported from s_1 to s_3 introduces a time delay in the dynamo process.

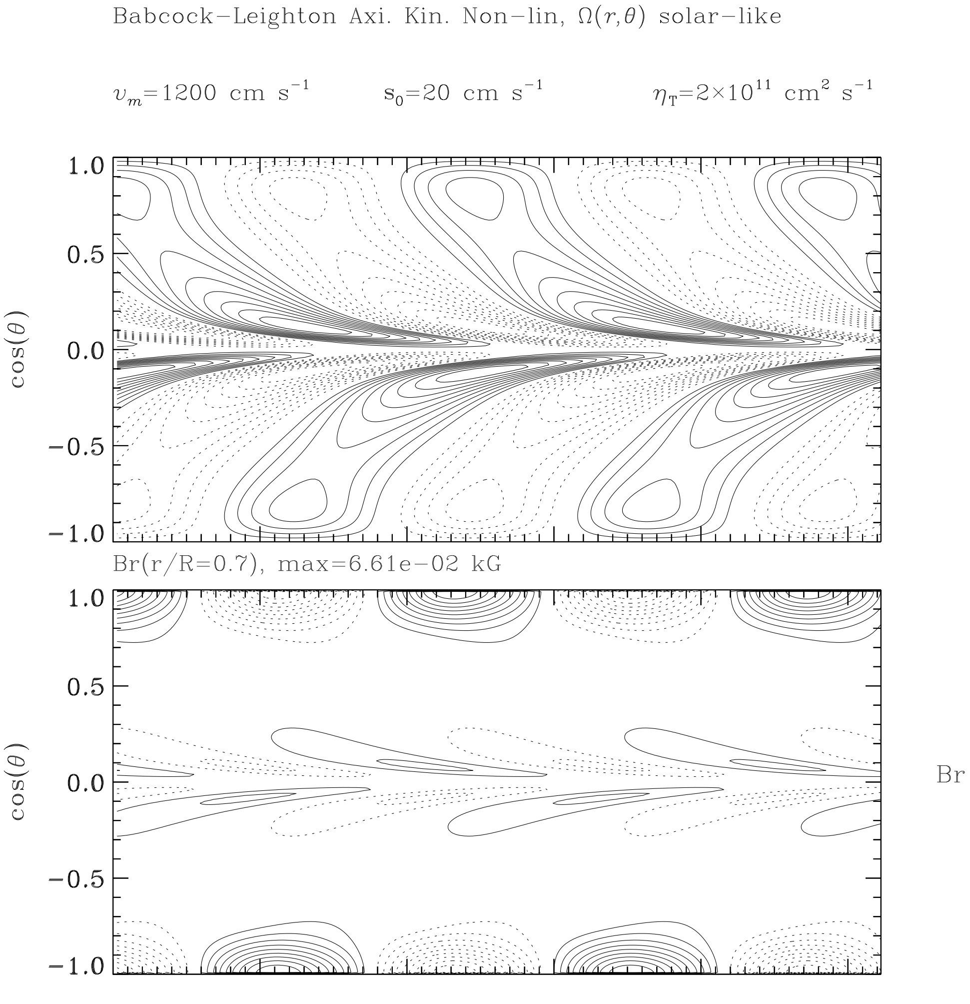

Figure 1.5: [F6.5] Butterfly diagrams for the solar-like Babcock-Leighton dynamo solution described in the text (solar-like differential rotation and meridional circulation, $\eta_T = 3 \times 10^{11}\,\mathrm{cm}^2\,\mathrm{s}^{-1}$, $C_\Omega = 47000$, $C_S = 4.64$, and $\mathrm{R}_m = 348$). Part (A) is the usual toroidal field butterfly diagram constructed at the core-envelope interface, and (B) is a surface butterfly diagram for the radial magnetic field component. Note the poleward migration and strong polar concentration of the radial component. Contour spacings as on Fig. **??**.

Figure 1.6: [F6.7] (A) Toroidal butterfly diagrami, and (B) time series of B^2, both extracted at the core-envelope interface, and the latter at 15° latitude (dotted line on part (A)). This is a strongly fluctuating solution, yet the dynamo continues to operate.

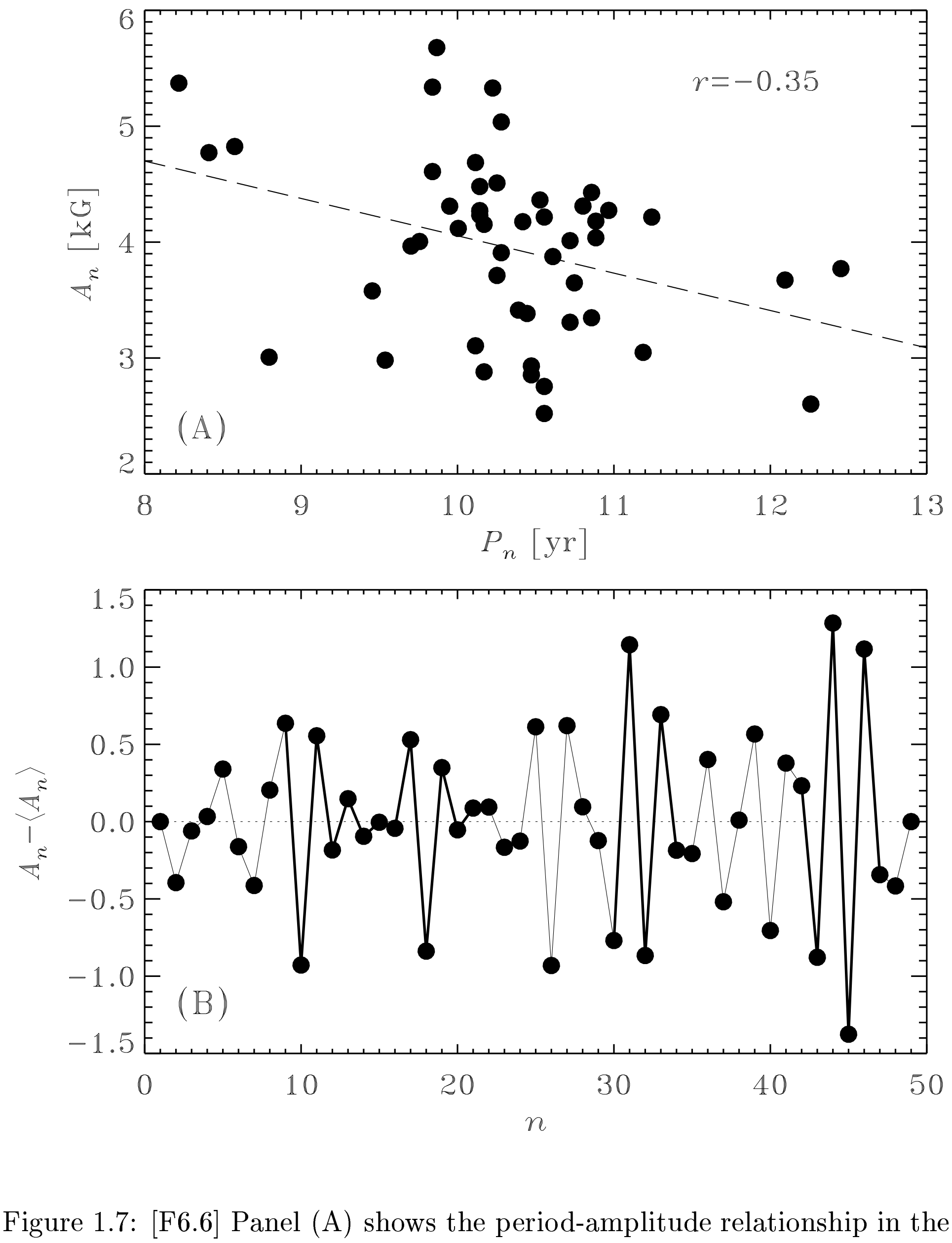

Figure 1.7: [F6.6] Panel (A) shows the period-amplitude relationship in the stochastically forced Babcock-Leighton dynamo solution described in the text. A linear least-square fit (dashed line) yields a linear correlation coefficient $r = -0.35$ which, why not particularly impressive, is comparable to that characerizing the period-amplitude anticorrelation of the sunspot record. Not also how the spread in period, 4–5 years, is also comparable to sunspot data. Panel (D) shows the sequence of detrended cycle amplitudes. The thicker line segments highlights the portions of the sequence where an off-even signal is present.

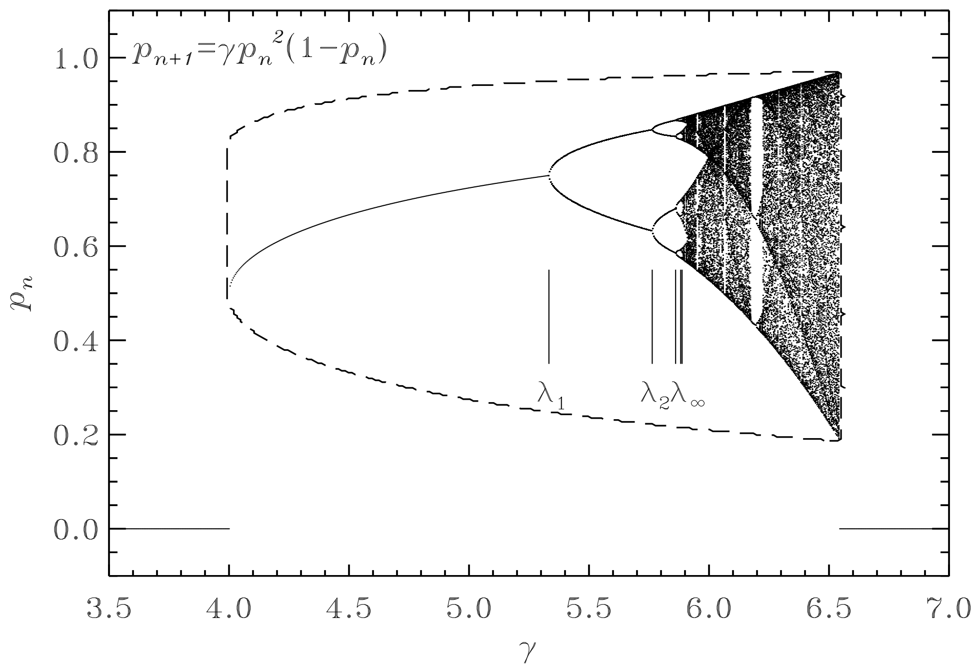

Figure 1.8: [F6.11] Bifurcation diagram for the map defined by eq. (1.27). The vertical line segments indicate the values of $\gamma = \lambda_m$ at which the first few bifurcations occur, as well as the value $\gamma \to \lambda_\infty = 5.8878$ at which transition to chaos takes place. The dashed line delineates the attraction basin boundary between the trivial solution $p_n = 0$ and the attractor. Non-trivial behavior is now restricted to the range $4.0000 \leq \gamma \leq 6.5433$, outside of which the only stable state is $p_n = 0$. Moreover, even within this range the trivial solution $p_n = 0$ still retains a basin of attraction of finite measure, corresponding to the region located outside of the closed dashed line.

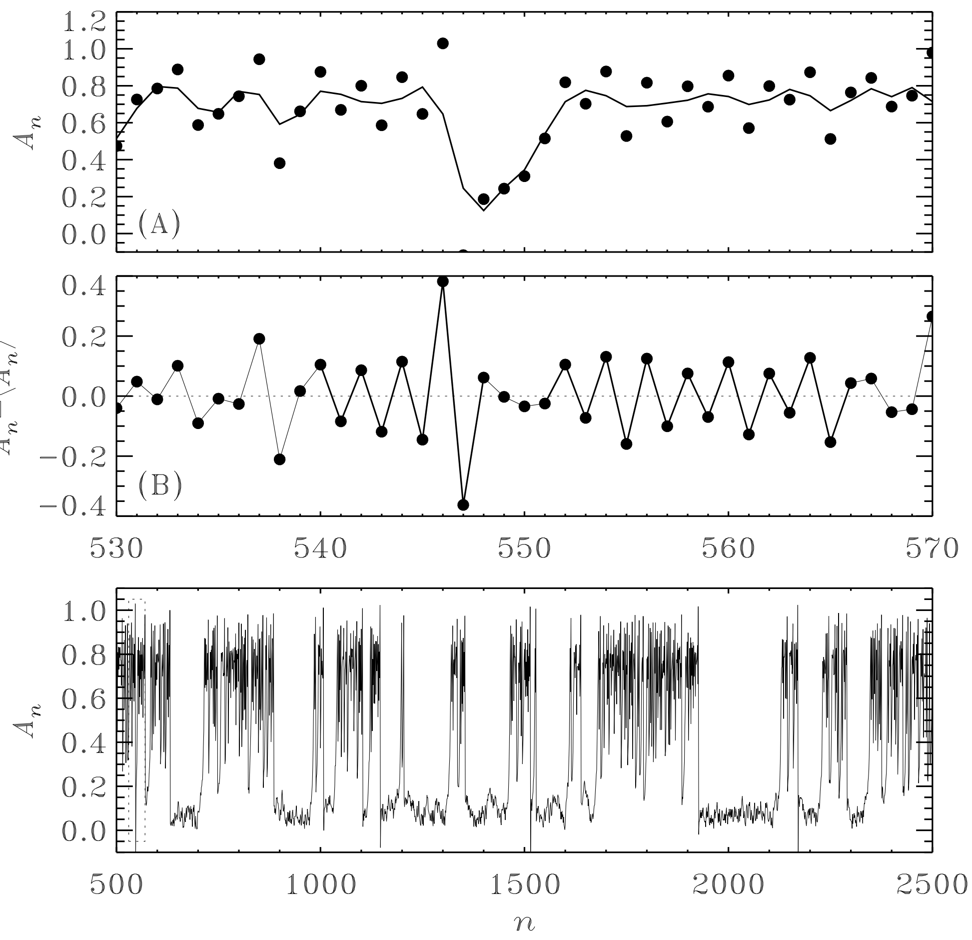

Figure 1.9: Portion of an amplitude iterate sequence for a stochastically forced version of eq. (1.33), with $\gamma \in [4.5, 6.5]$ and $\varepsilon_n \in [0, 0.09]$. Part (A) is the raw iterate sequence, with the thick line corresponding to a 1-2-1 running mean, while part (B) is the detrended sequence. Notice the persistence of the odd-even effect from iteration 540 to 547 and 551 to 566. Part (C) is a much longer sequence, showing the existence of intermittency in this stochastically forced map. The dotted box indicate the portion of the sequence plotted on panels A and B.